TABLE 1 Ranges of zonal temperature deviation profiles

Pressure (mbar)	10^{27} erg Day 1 ΔT(K)	10^{27} erg Day 2 ΔT(K)	10^{28} erg Day 1 ΔT(K)	10^{28} erg Day 2 ΔT(K)	10^{29} erg Day 1 ΔT(K)	10^{29} erg Day 2 ΔT(K)	10^{30} erg Day 1 ΔT(K)	10^{30} erg Day 2 ΔT(K)
Stratospheric energy deposition (16–69-mbar layer)								
16	0.02	0.06	0.1	0.1	0.4	0.6		
69	0.04	0.09	0.4	0.2	1.2	0.7		
287	0.02	0.08	0.2	0.1	0.7	0.5		
1,197	0.009	0.07	0.1	0.1	0.3	0.2		
5,000	0.004	0.03	0.04	0.04	0.1	0.08		
Tropospheric energy deposition (287–1,197-mbar layer)								
16	0.004	0.02	0.01	0.04	0.07	0.04	0.3	0.3
69	0.009	0.02	0.04	0.07	0.3	0.1	0.4	0.4
287	0.009	0.03	0.04	0.1	0.2	0.1	0.5	0.3
1,197	0.01	0.04	0.06	0.2	0.06	0.1	0.3	0.9
5,000	0.007	0.02	0.02	0.05	0.1	0.1	0.7	0.8

All our simulations show both a set of globally-propagating inertia-gravity waves and a longer-lived vortex at the impact site (see Fig. 2). Vortex behaviour depends on local conditions, but in our longest-run case (10^{28} erg, stratospheric deposition, 36 d) the vortex sheared into two components that moved west-northwest and east-southeast. In all simulations inertia-gravity waves travel at ~400 m s^{-1} in the stratosphere and slower in the troposphere. There is an antipodal wave crossing, but no single focus of energy because of wave dispersion and Jupiter's oblateness. Because there is less mass and stronger stratification, stratospheric deposition excites stronger waves than tropospheric deposition (see Fig. 1). Table 1 contains each simulation's temperature deviation range. The waves interfere with one another behind the first wavefront, making it difficult to determine the functional form of the increase of temperature range ΔT with comet energy, although it is not faster than linear.

Observers can probe different atmospheric levels by selecting wavelengths that are sensitive to different regions. The predicted temperature deviations caused by Shoemaker–Levy 9 inertia-gravity waves bracket the detection threshold for thermal infrared imaging, which probes the stratosphere[22–24]. Transient condensation effects similar to those seen in mountain lee waves may be visible in high-resolution, reflected-light images of the waves' horizontal passage through the ammonia clouds (upper troposphere). Whether such effects are indeed seen will depend upon local circumstances and the size of the wave. Inertia-gravity waves will be distinguishable from seismic waves[19] by the former's slower propagation rate and stronger thermal signature. Observers should be careful not to confuse the remnant signatures of seismic effects close to the impact sites with those of propagating inertia-gravity waves. In all cases, techniques that take advantage of the waves' circular coherence (see Fig. 2), such as averaging in radial bins around the impact locations, will improve the signal-to-noise ratio of the wave trace. Because of the uniqueness of this event and the potential for significant improvements in dynamical modelling, observers should attempt to determine inertia-gravity wave speeds at as many pressure levels as possible. □

Received 14 December 1993; accepted 3 March 1994.

1. Nakano, S. *IAU Circ. No.* 5800 (1993).
2. Carusi, A. & Yeomans, D. K. *IAU Circ. No.* 5807 (1993).
3. Chodas, P. W. & Yeomans, D. K. *Bull. Am. Astr. Soc.* **25,** 1042–1043 (1993).
4. Dowling, T. E. *Bull. Am. Astr. Soc.* **25,** 1031 (1993).
5. Scotti, J. V. & Melosh, H. J. *Nature* **365,** 733–735 (1993).
6. Weaver, H. A. *et al. Science* **263,** 787–791 (1994).
7. Sekanina, Z. *Science* **262,** 382–387 (1993).
8. Zahnle, K. & Mac Low, M.-M. *Icarus* (in the press).
9. Conrath, B. J., Gierasch, P. J. & Nath, N. *Icarus* **48,** 256–282 (1981).
10. Dowling, T. E. & Ingersoll, A. P. *J. atmos. Sci.* **46,** 3256–3278 (1989).
11. Ingersoll, A. P. & Cuong, P. G. *J. atmos. Sci.* **38,** 2067–2076 (1981).
12. Marcus, P. S. *Nature* **331,** 693–696 (1988).
13. Williams, G. P. & Wilson, R. J. *J. atmos. Sci.* **45,** 207–241 (1988).
14. Melosh, H. J. & Schenk, P. *Nature* **365,** 731–733 (1993).
15. Hsu, Y.-J. G. & Arakawa, A. *Mon. Weath. Rev.* **118,** 1933–1959 (1990).
16. Dowling, T. E. *J. atmos. Sci.* **50,** 14–22 (1993).
17. Pirraglia, J. A., Conrath, B. J., Allison, M. D. & Gierasch, P. J. *Nature* **292,** 677–679 (1981).
18. Limaye, S. S. *Icarus* **65,** 335–352 (1986).
19. Marley, M. S. *Astrophys. J. Lett.* (in the press).
20. Klemp, J. B. & Lilly, D. K. *J. atmos. Sci.* **35,** 78–107 (1978).
21. Ahrens, T. J., Takata, T. & O'Keefe, J. D. *Bull. Am. Astr. Soc.* **25,** 1043 (1993).
22. Deming, D. *et al. Astrophys. J.* **343,** 456–467 (1989).
23. Gezari, D. Y. *et al. Nature* **342,** 777–780 (1989).
24. Orton, G. S. *et al. Science* **252,** 537–542 (1991).

ACKNOWLEDGEMENTS. We thank E. Charrette and the MIT Earth Resources Laboratory for programming assistance and use of their nCUBE 2 massively parallel computer. This work was funded by NASA.

Trapped electron acceleration by a laser-driven relativistic plasma wave

M. Everett, A. Lal, D. Gordon, C. E. Clayton, K. A. Marsh & C. Joshi

Department of Electrical Engineering, University of California at Los Angeles, Los Angeles, California 90024, USA

THE aim of new approaches for high-energy particle acceleration[1] is to push the acceleration rate beyond the limit (~100 MeV m^{-1}) imposed by radio-frequency breakdown in conventional accelerators. Relativistic plasma waves, having phase velocities very close to the speed of light, have been proposed[2–6] as a means of accelerating charged particles, and this has recently been demonstrated[7,8]. Here we show that the charged particles can be trapped by relativistic plasma waves—a necessary condition for obtaining the maximum amount of energy theoretically possible for such schemes. In our experiments, plasma waves are excited in a hydrogen plasma by beats induced by two collinear laser beams, the difference in whose frequencies matches the plasma frequency. Electrons with an energy of 2 MeV are injected into the excited plasma, and the energy spectrum of the exiting electrons is analysed. We detect electrons with velocities exceeding that of the plasma wave, demonstrating that some electrons are 'trapped' by the wave potential and therefore move synchronously with the plasma wave. We observe a maximum energy gain of 28 MeV, corresponding to an acceleration rate of about 2.8 GeV m^{-1}.

Relativistic plasma waves are particularly useful for accelerating particles for two reasons. First, the electric fields within these waves can be extremely high. Second, the fact that these waves can be made to move at the same speed as a highly relativistic particle means that the accelerating particles will interact with the fields for a long time, and can thus be accelerated to very high energies. In this 'plasma beat-wave accelerator' experiment, such a wave is driven by illuminating a suitable plasma with two laser beams of slightly different frequencies. The interference—or beating—of the two beams exerts a force on the plasma at the difference frequency $\Delta\omega$ and difference wavenumber Δk, thus modulating the plasma density. The electric field of the wave is just the space-charge field associated with this modulated electron density as one would find from Gauss's law.

Over the last decade, many groups have reported success in the excitation of relativistic plasma waves using the 'beat-wave' technique[9–11]. More recently, acceleration of externally injected[7] as well as background plasma electrons[8] by beat-excited plasma waves has also been shown. But in order to make a useful device based on this scheme, not only must electrons be injected externally into such a wave, they must be 'trapped' by the wave potential[12]. Although trapping is not a necessary condition for some energy gain, only the trapped electrons can gain the theoretical maximum amount of energy limited by dephasing which occurs when the polarity of the electric field of the plasma wave

changes its sign. A trapped electron, by definition, moves synchronously with the wave at the point of reflection in the wave potential. At this point the trapped electron has a relativistic Lorentz factor $\gamma_{ph}=(1-v_{ph}^2/c^2)^{-1/2}$ where v_{ph} is the phase velocity of the wave. Thereafter, as the electron continues to gain energy, it remains trapped and executes a closed orbit in the wave potential. Trapping tends to bunch the electrons in phase space resulting in a relatively narrow energy spread, which is necessary for most applications. Trapped electrons bunch in physical space because the trailing electrons see a higher field than the leading electrons and tend to catch up with the latter. This bunching then leads to a narrow energy spectrum as all the electrons subsequently interact with roughly the same accelerating field. If the initial electron energy is less than $0.511(\gamma_{ph}-1)$ MeV (the kinetic energy of an electron moving synchronously with the wave), observation of accelerated electrons with energies greater than this indicates acceleration of trapped electrons by the wave. Here we present the first evidence of such trapped particle acceleration of externally injected electrons by a relativistically propagating plasma wave.

The experimental parameters and the apparatus has been discussed in detail elsewhere[13]. A two-frequency CO_2 laser beam (10.28 μm and 10.59 μm wavelengths, 150 ps rise time and 5×10^{14} W cm^{-2} peak intensity) and a co-propagating 2-MeV electron beam are both focused to the same point in a vacuum chamber filled with ~155 mT of hydrogen. The gas pressure is chosen so that the difference frequency between the two laser lines $\Delta\omega$ equals the plasma frequency ω_p of the laser-ionized gas. This plasma frequency corresponds to a plasma-wave wavelength of only 0.34 mm. On full ionization, the plasma wave grows rapidly in time and some of the injected electrons are trapped and accelerated. The injected electrons have a full width at half maximum (FWHM) spot size of 250 μm whereas the laser spot size is ~180 μm (FWHM). The average electron current over the 1.5 ns (FWHM) macropulse is 25 mA. This macropulse has a microstructure at 9.3 GHz, with each micropulse ~10 ps (FWHM) in duration, giving a peak current of 270 mA. Because the macropulse is much longer in duration than the excited plasma wave, most of the injected electrons are unaffected by the plasma wave. These electrons are dumped onto low-density plastic. The accelerated electrons leave the vacuum through a 25-μm-thick Mylar window and are detected electronically by one or more silicon surface barrier detectors or by a gaseous Cherenkov cell followed by a photomultiplier tube. Electrons are also detected photographically by the tracks they leave in a cloud chamber[7].

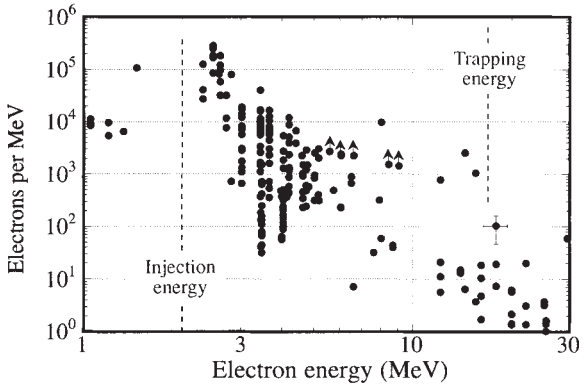

FIG. 1 The cumulative energy spectrum of electrons leaving the plasma wave within a full cone angle of 6°. To obtain this data, various charge-sensitive preamplifiers and thick-lead apertures were used to extend the dynamic range of the electron detectors to over four orders of magnitude in electron flux beginning with single-electron sensitivity. The energy dispersion across the aperture of the detector was considered in arriving at the plotted electrons per MeV. The points with arrows are lower bounds due to detector saturation. At a given setting of the electron-spectrometer magnetic field, data can only be obtained at three energies per laser shot. Therefore, a complete electron spectrum has to be accumulated over many shots. The dashed lines mark the injection energy and the trapping, where the latter refers to the energy which the electrons must have to move synchronously with the plasma wave.

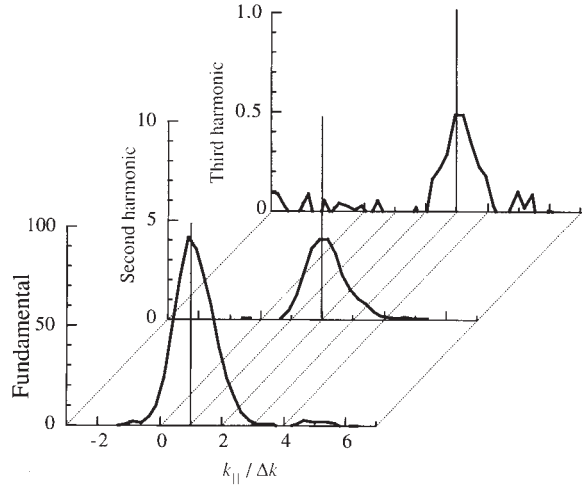

FIG. 2 Signals at $\Delta\omega$, $2\Delta\omega$ and $3\Delta\omega$ taken from the time-integrated frequency–wavenumber spectrum of the plasma wave obtained by small-angle Thomson scattering. The width of each peak is instrument-limited; the height is given in arbitrary units. Because the wavelength of the plasma wave and its radial extent are comparable, the plasma wave has a broad perpendicular wavenumber ($k_\perp$) spectrum. In the 90° scattering geometry used here, energy and momentum can only be conserved[17] for photons that scatter from the component of the wave with $k_\perp=k_\parallel$ ($=m\Delta k$ for the mth harmonic scattered order). From knowledge of the laser spot profile, we estimate the $k_\perp$ spectrum of the plasma wave and thereby quantify the relative amplitude of each wave harmonic[18].

The two main diagnostics are an electron energy spectrometer and 'small-angle' Thomson scattering[14,15]. A complete spectrum of electrons that are accelerated—as well as those decelerated (because they see an electric field of the wrong polarity)—by the plasma wave is shown in Fig. 1. The large scatter in the absolute number of electrons in a given energy bin is due both to the timing jitter (±50 ps) between the injected electron bunch and the plasma wave, and to the shot-to-shot variation in the laser pulses. The lifetime of the accelerating fields estimated from the optical measurements described below is ~50 ps (FWHM). Thus the points that give the maximum number of electrons at a given energy probably correspond to perfect synchronism of the injected electrons with the peak plasma wave fields. The jitter also contributes to the large energy spread observed in the spectrum. Another contributing factor to the spread is that the electrons are not pre-bunched into the ideal phases of the wave. The plasma wave period is ~1 ps whereas the electron bunch is about 10 ps and therefore the injected electrons uniformly occupy all phases over ~10 plasma oscillations. In these experiments the plasma wave has a Lorentz factor γ_{ph} of ~33 which would be synchronous with a 16-MeV electron. Therefore all the observed electrons with energies above 16 MeV are indeed trapped electrons and are thus moving forward in the frame of the wave.

The maximum electron energy gives an upper bound on the longitudinal electric field of the wave integrated along the electron trajectory through the wave. Because (as discussed earlier) the electric field is the space-charge field arising from plasma density perturbations of the wave, optical Thomson scattering

can be used to measure these density perturbations and obtain information about the wave electric fields independent of the energy gain measurement. Essentially, the density perturbations look like a moving volume grating which can diffract the probe beam into frequency-shifted 'orders'. The 2-ns (FWHM), 50-MW, 0.53-μm optical probe beam (ω_{pr}, k_{pr}) traverses the plasma wave at a right angle to its direction of propagation. In this configuration, the probe beam has a cylindrical focus 6 mm (~20 plasma wavelengths) long. The scattered light is observed to be emitted at various discrete angles $\theta = k_{\parallel}/k_{pr}$ (where $k_{\parallel} = m\Delta k$) and frequency-shifted by $\omega_{pr} - m\omega_p$. Here $k_{\parallel}$ is the wavenumber of the mth harmonic of the plasma wave along the propagation direction of the electron beam and Δk is the wavenumber difference between the two laser beams. Figure 2 shows the time-integrated ω–k spectrum of the density perturbations of the wave obtained by Thomson scattering. This spectrum clearly shows discrete peaks at ($m\Delta\omega$, $m\Delta k$) for $1 \leqslant m \leqslant 3$ corresponding to scattering of light from the fundamental and second and third harmonics of the relativistic plasma wave. Using nonlinear wave theory[16], which gives the normalized amplitude of the mth harmonic a_m as a function of the normalized amplitude of the fundamental a_0 as $a_m \approx a_0^m$, one can obtain an estimate of the plasma wave amplitude based on its harmonic content. After correcting for the finite-$k_{\perp}$ effects[17,18], we obtain an estimate for the density perturbation of 38% of the background density (based on the second-harmonic to fundamental ratio), or 40% (from the third-harmonic to fundamental ratio). Alternatively, we can obtain an amplitude estimate based on the absolute intensity of the scattered light from which we infer a 30% wave amplitude. This latter estimate agrees well with two-dimensional 'particle-in-cell' computer simulation of our exact experimental parameters. We can compare these optical measurements to the electron measurements by noting that the interaction length for our focusing conditions is expected to be ~1.0 cm (ref. 19). Thus, the 30-MeV electrons gained energy at a rate of 2.8 GeV m^{-1} which, from Gauss's law, corresponds to a wave amplitude of 28%, in good agreement with the independent optical diagnostic and the computer simulation. A more theoretical discussion of the acceleration and scattering of electrons observed in our experiments will be presented elsewhere[19]. □

Received 15 November 1993; accepted 22 February 1994.

1. Sessler, A. M. *Physics Today* **41,** 26–34 (1988).
2. Dawson, J. M. *Scient. Am.* **260,** 54–61 (1989).
3. Trajima, T. & Dawson, J. M. *Phys. Rev. Lett.* **43,** 267–270 (1979).
4. Sprangle, P., Esarey, E., Ting, A. & Joyce, G. *Appl. Phys. Lett.* **53,** 2146–2148 (1988).
5. Chen, P., Dawson, J. M., Huff, R. W. & Katsouleas, T. *Phys. Rev. Lett.* **54,** 693–696 (1985).
6. Joshi, C. *et al. Nature* **311,** 525–529 (1984).
7. Clayton, C. E. *et al. Phys. Rev. Lett.* **70,** 37–40 (1993).
8. Kitagawa, Y. *et al. Phys. Rev. Lett.* **68,** 48–51 (1992).
9. Clayton, C. E., Joshi, C., Darrow, C. & Umstadter, D. *Phys. Rev. Lett.* **54,** 2343–2346 (1985).
10. Amiranoff, F. *et al. Phys. Rev. Lett.* **68,** 3710–3713 (1992).
11. Dangor, A. E., Dymoke-Bradshaw, A. K. L. & Dyson, A. E. *Physica Scripta* **T30,** 107–109 (1990).
12. Williams, R. L., Clayton, C. E., Joshi, C., Katsouleas, T. & Mori, W. B. *Lasers Particle Beams* **8,** 427–449 (1990).
13. Joshi, C. *et al. Advanced Accelerator Concepts* 379–410 (AIP Conf. Proc. No. 279, Amer. Inst. Phys., New York, 1993).
14. Sheffield, J. *Plasma Scattering of Electromagnetic Radiation* (Academic, New York, 1975).
15. Clayton, C. E., Darrow, C. & Joshi, C. *Appl. Opt.* **24,** 2823–2826 (1985).
16. Jackson, E. A. *Phys. Fluids* **3,** 831–833 (1960).
17. Martin, F., Johnston, T. W. & Ebrahim, N. *Phys. Rev. Lett.* **55,** 1651 (1985).
18. Clayton, C. E., Joshi, C., Darrow, C. & Umstadter, D. *Phys. Rev. Lett.* **55,** 1652 (1985).
19. Clayton, C. E. *et al. Phys. Plasmas* (in the press).

Emission of blue light from hydrogenated amorphous silicon carbide

W. A. Nevin, H. Yamagishi, M. Yamaguchi & Y. Tawada

Central Research Laboratories, Kaneka Corporation, 1-2-80, Yoshida-cho, Hyogo, Kobe 652, Japan

THE development of new electroluminescent materials is of current technological interest for use in flat-screen full-colour displays[1]. For such applications, amorphous inorganic semiconductors appear particularly promising, in view of the ease with which uniform films with good mechanical and electronic properties can be deposited over large areas[2]. Luminescence has been reported[1] in the red-green part of the spectrum from amorphous silicon carbide prepared from gas-phase mixtures of silane and a carbon-containing species (usually methane or ethylene). But it is not possible to achieve blue luminescence by this approach. Here we show that the use of an aromatic species—xylene—as the source of carbon during deposition results in a form of amorphous silicon carbide that exhibits strong blue luminescence. The underlying structure of this material seems to be an unusual combination of an inorganic silicon carbide lattice with a substantial 'organic' π-conjugated carbon system, the latter dominating the emission properties. Moreover, the material can be readily doped with an electron acceptor in a manner similar to organic semiconductors[3], and might therefore find applications as a conductivity- or colour-based chemical sensor.

The hydrogenated amorphous silicon carbide (a-$Si_{1-x}C_x$:H) films were deposited from mixtures of xylene (C_8H_{10}, Fig. 1 inset) and silane (SiH_4). Figure 1 shows the infrared spectra of three films, fabricated using different compositions of reaction gas mixture. Vibrational modes typical of those found in a-$Si_{1-x}C_x$:H prepared from conventional nonaromatic carbon sources, such as methane[4], are seen. These are characteristic of an inorganic lattice, where silicon and carbon are tetrahedrally coordinated in a covalent sp^3-bonded system, with hydrogen acting as a network terminator in the form of CH_n and SiH_n groups[5]. As expected, the ratio of the intensities of the C–H to Si–H modes decreases with decreasing xylene gas fraction (and hence, x), in the order of Fig. 1*a*–*c*. In addition, the presence of large amounts of π-bonded carbon is indicated by the occurrence of strong absorption due to sp^2 C–H stretching and sp^2 C=C stretching modes[6]. The sharpness of these modes and the occurrence of additional sharp peaks in the region of 600–800 cm^{-1}, at positions similar to those of pure xylene, implies that the bulk of the sp^2-carbon sites are in the form of relatively isolated aromatic rings having a high degree of bonding to hydrogen. This is in marked contrast to films prepared from conventional sources, where the C–H modes consist almost entirely of sp^3-carbon sites, and although an increasing amount of sp^2 carbon is seen at contents above $x \approx 0.6$, this has an unhydrogenated, fused-ring, graphitic-type structure[4,5]. It should be noted that our films do also contain some olefinic and/or fused aromatic structure, shown by the presence of a broad underlying absorption in the sp^2 C–H and C=C stretching regions[6].

The optical band gap (E_{opt}) for the range of films prepared is plotted as a function of carbon content in Fig. 2. Two approximately linear regions are seen with a change to a steeper slope at $x \approx 0.75$. This is in good agreement with theory, which predicts an increase in slope when the band edges change from Si-like to SiC-like as x increases[5]. In contrast, in films prepared from conventional sources, E_{opt} generally reaches a maximum value of <3.0 eV at $x \approx 0.60$, then decreases[5]. This decrease is thought to result from a change in the band-edge character from one controlled by the σ-bonded SiC lattice to a (π–π^*) orbital-type gap, related to the increasing presence of sp^2 graphitic clusters. The (π–π^*) band gap is expected to decrease with increasing